PROCEEDINGS A

rspa.royalsocietypublishing.org

Research

Cite this article: Mihai LA, Alayyash K, Goriely A. 2015 Paws, pads and plants: the enhanced elasticity of cell-filled load-bearing structures. *Proc. R. Soc. A* **471**: 20150107. http://dx.doi.org/10.1098/rspa.2015.0107

Received: 17 February 2015
Accepted: 30 April 2015

Subject Areas:
applied mathematics, mathematical modelling

Keywords:
constitutive behaviour, cellular structures, elastic material, large strain, finite elements, soft tissue

Author for correspondence:
L. Angela Mihai
e-mail: mihaila@cardiff.ac.uk

Paws, pads and plants: the enhanced elasticity of cell-filled load-bearing structures

L. Angela Mihai[1], Khulud Alayyash[1] and Alain Goriely[2]

[1]School of Mathematics, Cardiff University, Senghennydd Road, Cardiff CF24 4AG, UK
[2]Mathematical Institute, University of Oxford, Woodstock Road, Oxford OX2 6GG, UK

Paws, fat pads and plants share a remarkable structure made up of closed cells with elastic cell walls capable of supporting large loads and deformations. A key challenge is to understand how the function of these structures is enhanced by their geometric and material design. To do so, we compare different elastic models operating in large strain deformation when the cells are empty or filled with an incompressible liquid or solid core. We demonstrate theoretically, for three different cell geometries, that the elastic modulus in a direction associated with the change of curvature in the cell wall (i) is greater when the cell is filled; (ii) increases as the internal cell pressure increases; and (iii) increases also as the thickness of the cell wall increases or when the wall is multi-layer. As these results do not depend on the choice of the strain-energy function describing the cell-wall material, they are valid for a wide range of structures made from different elastic materials. For multiple cells deforming together due to external forces, the increase in elastic modulus of the cell walls under increasing core pressure is found numerically throughout the structure.

1. Introduction

Paw and plantar pads are nature's wonders of design. They are protective, load-bearing structures, without which balanced stand and independent walk in humans and many non-human mammals would not be possible.

THE ROYAL SOCIETY PUBLISHING

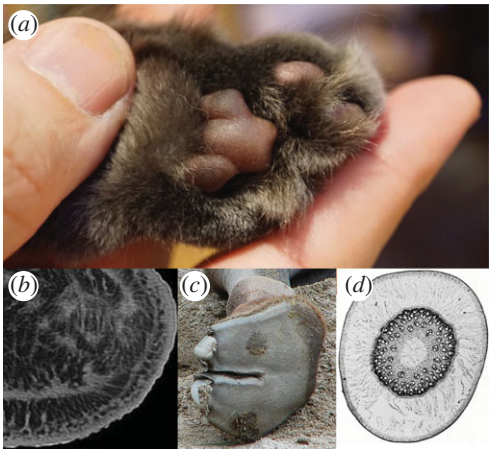

Figure 1. (*a*) Cat paw pads (image courtesy of Z. Goriely); (*b*) CT image of the hindlimb of an African elephant showing fibrous and adipose tissues in foot cushion [1]; (*c*) camel foot pad; (*d*) cross section of the stem of *Distichlis spicata* [2]. (Online version in colour.)

The soft padding of a cat's paws (figure 1) is the more obvious example, but the Arabian camel (*Camelus dromedarius*) too relies on a wide fat pad that connects its toes preventing it from sinking into the sand, and allowing it to make almost no sound when walking or running [3]. Indeed, all members of the *Camelidae* family (including camels, llamas, alpacas, vicuñas and guanacos) are extant representatives of the suborder Tylopoda (Latin for 'padded foot'). The African elephant (*Loxodonta africana*) also has large foot cushions that expand medially, laterally and palmarly/plantarly when compressed [1]. In humans, the average maximal deformation of the heel pad is approximately 35.5% (approx. 5.3 mm) of its thickness, 60% (approx. 9 mm) while running barefoot and 25% (approx. 3.75 mm) upon weight bearing [4,5]. Despite their exceptional resilience, damage to heel pads can lead to clinical conditions ranging from shock-induced heel pain to musculo-skeletal injuries to chronic disorders and disability [5].

Histologically, paw and foot cushions are soft cellular bodies built from closed compartments or cells separated by collagen reinforced elastic septa and filled with fat (adipose tissue) [1,3,6,7]. As part of the locomotor system, they are designed to absorb mechanical shock, redistribute excessive local stress, and store and return elastic strain energy. In particular, the septa in the heel pad are U- or comma-shaped columns arranged in a mostly vertical orientation designed to resist compression. When the heel is subject to vertical compression, after an initial displacement, the collagen-reinforced septa, which are under tension in the lateral and antero-dorsal directions, straighten and become taut, limiting the deformation of the heel tissue, while the volume of the fat-filled interior remains constant. If the septa walls become thicker or more fibrous, then they become more difficult to stretch and deform under loading, while if the walls break down, then the structure becomes more easily deformed resulting in an atrophic pad [5,8,9]. Experimental tests show a strong nonlinearity of the mechanical response of the fat pad under compression and visco-elastic models have been proposed to account for this behaviour [10–12]. The function of pads relies crucially on the biomechanics and deformation of individual cells. In particular, it depends both on the mechanical response of the cell walls and the geometric constraint on the deformation provided by the closed cell.

We carry out a systematic theoretical comparison of the mechanical performance for individual cell walls made from an homogeneous, incompressible, isotropic, hyperelastic material in a single cell which is either empty or filled with an incompressible fluid or a compliant, elastic core and subject to large strain deformations. We consider three general cell types (made out of straight edges, curved edges or cylindrical) made from a homogeneous, isotropic, hyperelastic material

that satisfies both the Baker–Ericksen (BE) inequalities stating that *the greater principal stress occurs in the direction of the greater principal stretch*, and of the pressure-compression (PC) inequalities stating that *each principal stress is a pressure* (*compression*) *or a tension according as the corresponding principal stretch is a contraction or an elongation* (*extension*) [13, pp. 155–159]. These inequalities are valid for most isotropic elastic materials, and their suitability to model biological and cellular materials is discussed in [14,15].

Other natural cellular structures such as sponges and plant stems maintain their integrity under loading by internal strengthening of cell walls either through fibre reinforcement or by thickening of the walls in load-bearing regions [16–18]. For example, monocotyledon stems (e.g. corn, palms, bamboos) prevent mechanical failure through a combination of initiation of growth with an 'overbuilt' stem that is sufficiently wide for future support demands, and sustained sclerification (thickening and lignification) of cell walls towards the stem periphery and base [19]. Our analysis for the deformation of cylindrical cell walls also provides key insight in the mechanical response of these structures [20].

For biogenic cellular structures in general, physical evidence shows that several main factors determine the magnitude of the enhancement of stress level in the cellular material, involving the individual cell geometry, the cell wall thickness, and the presence of cell inclusions [16,21]. These competing elastic properties play a significant role in the manner in which natural cellular materials are designed to achieve their superior structural performance. For example, in plant stems, turgor pressure induces stretching in the parenchyma cell walls, while the mechanical properties of cartilage depend on osmotic pressure developed within an aqueous proteoglycan gel and resisted by tension in a collagenous network [17].

In the case of small strain deformations, a comparison between empty and fluid-filled cells was proposed by [21], where it was shown that, if a cell wall is bent, then the elastic modulus in the direction of the force causing the deflection increases in a fluid-filled cell compared with that of an empty cell. Indeed, if the underlying material is linearly elastic, then the dominant mechanism for the deformation of a cellular body is the bending of the cell walls [22]. However, in soft cushioning structures, large strain deformations occur, and particular care must be taken for these situations [23].

Here, we establish general comparison principles between empty and filled cells for three cell-wall geometries based on the *nonlinear elastic modulus* representing the ratio between the values of the stress and the strain in the direction associated with the largest change of curvature in the deforming walls. Since the deformations analysed here can be maintained in every homogeneous, isotropic, incompressible, hyperelastic body by application of suitable tractions, *these comparison principles are universal in the sense that they are derived independently of the choice of the strain-energy function for the cell wall material*. We show that, for a rectangular wall which is bent into an annular wedge the elastic modulus in the radial direction of the deformed wall is greater when the cell is closed and filled with an incompressible core than when the cell is open (§2a). Similarly, for an annular wedge which is straightened into a rectangular wall, the elastic modulus in the transverse directions is greater in the closed cell than in the open cell (§2b). For a circular tube which is stretched and twisted, we find that the elastic modulus in the radial direction of the tube wall is greater when the tube is closed at its ends and is filled with an incompressible core than when the tube is open (§2c). Furthermore, in our analysis, the dependence of the elastic modulus on the pre-stress due to the internal cell pressure is also established. By contrast, when the cell-wall material is linearly elastic, the elastic modulus of the cell wall is independent of initial cell pressure [22, p. 253].

For all these deformations, the elastic modulus of the cell wall further increases as the thickness of the wall increases or when the wall becomes multi-layer. In particular, for sandwich structures in bending, the stiffness of the middle layer, which acts as an elastic support for the adjacent layers, is found to be enhanced in part by the contact conditions with these layers. This property is not retained by sandwich structure made from linearly elastic materials [22, p. 350]. Similarly, if a circular tube is filled with an incompressible elastic core, then the radial elastic modulus of the cylindrical core is also enhanced by the contact with the surrounding tube.

For assemblies of cells deforming under external forces, numerical models also show that the average elastic modulus of the cell walls in the direction of the applied force is greater when the cells are filled with an elastic core than when the cells are empty, and increases as the pressure in the cell core increases (§3). This is in agreement with the theoretical results for the pre-defined deformations, and represents an extension of those results to the more general deformations of the model structures.

Even though natural cellular structures are irregular, and their properties and behaviour are constantly adapting to internal and external conditions, our results indicate that the cell inclusion in a geometrically closed cell plays a twofold role: on the one hand, it maintains the integrity of the deforming structure by preventing densification or compaction, and, on the other hand, it enhances the stiffness of the cell walls through additional local constraints. Furthermore, although cellular materials do not resist standard elastic deformations, such as bending, stretching or twisting, the stress attained at a given value of strain increases with the wall thickness. Since a reduction in the energy absorbing capacity of a cellular structure is typical when the cell-wall stiffness increases, these changes in the material properties play a significant role in the manner in which these structures perform their roles.

Our mechanical analysis addresses the need for a better understanding of cellular materials which are widespread in nature and in pharmaceutical and nutraceutical industries, and in particular, of paw and plantar fat cushions, and plants.

2. The nonlinear elastic modulus of cell walls

The deformations analysed in this section can be maintained in every homogeneous, incompressible, isotropic, elastic material by application of suitable surface tractions [13,24–26]. If the material is described by a strain-energy function $\mathcal{W}$, the associated Cauchy (true) stress has the Rivlin–Ericksen representation:

$$\boldsymbol{\sigma} = -p\mathbf{I} + \beta_1\mathbf{B} + \beta_{-1}\mathbf{B}^{-1},$$

where $\mathbf{B}$ is the left Cauchy–Green strain tensor, I_1, I_2, I_3 are principal strain invariants, p is an arbitrary hydrostatic pressure and

$$\beta_1 = 2\frac{\partial \mathcal{W}}{\partial I_1}, \quad \beta_{-1} = -2\frac{\partial \mathcal{W}}{\partial I_2}$$

are the material responses. Here we require the validity of the empirical inequalities:

$$\beta_1 > 0 \quad \text{and} \quad \beta_{-1} \leq 0.$$

Then the BE inequalities also hold [13, pp. 155–159].

(a) Rectangular walls

A cuboid cell wall with reference geometry $(X, Y, Z) \in [C_1, C_2] \times [-Y_0, Y_0] \times [-Z_0, Z_0]$, where C_1, C_2, Y_0 and Z_0 are positive constants, is deformed by the triaxial stretch

$$\tilde{X} = aX, \quad \tilde{Y} = \frac{1}{\sqrt{a}}Y \quad \text{and} \quad \tilde{Z} = \frac{1}{\sqrt{a}}Z, \tag{2.1}$$

where $(\tilde{X}, \tilde{Y}, \tilde{Z})$ and (X, Y, Z) are the Cartesian coordinates for the deformed and the reference configuration, respectively, and a is a positive constant. For this deformation, the only non-zero component of the Cauchy stress tensor is $\sigma^{(0)}_{\tilde{X}\tilde{X}} = -p_0$ (appendix A*a*). In the linear elastic limit, where $a \to 1$, $p_0 = 0$.

Then the deformed wall is bent into a sector of a circular cylindrical tube (annular wedge) by the deformation

$$r = \sqrt{2\tilde{X}}, \quad \theta = A\tilde{Y} \quad \text{and} \quad z = \frac{\tilde{Z}}{A}, \tag{2.2}$$

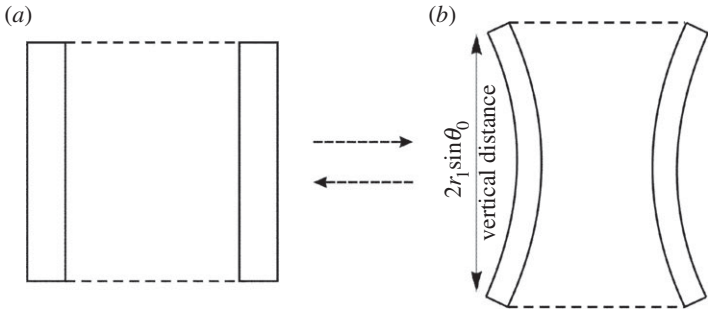

Figure 2. Schematic of finite bending (*a*) and straightening (*b*). The vertical distance between the ends of the wall may increase (closed, filled cell) or remain unchanged (open cell).

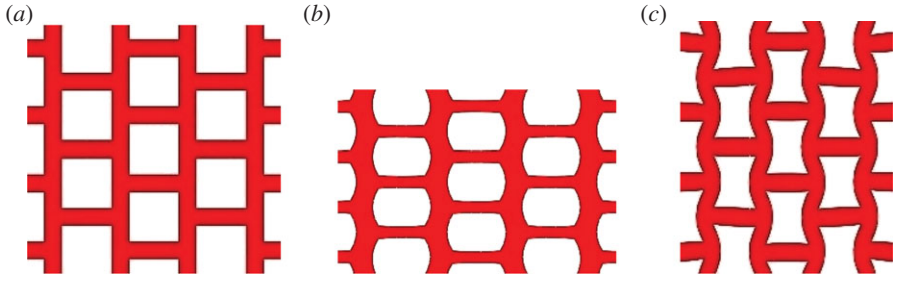

Figure 3. Sample of periodic cellular structure with cell walls that are (*a*) straight, (*b*) bent outside the cell or (*c*) bent inside the cell. (Online version in colour.)

where $(r,\theta,z)\in[r_1,r_2]\times[-\theta_0,\theta_0]\times[-z_0,z_0]$ are the cylindrical polar coordinates for the current configuration, and r_1, r_2, θ_0, z_0 and A are positive constants (figure 2).

The deformation (2.2) superposed on (2.1) is a suitable approximation for the bending cell walls in a periodic structure as illustrated schematically in figure 3. In this figure, the cross-section sample of a structure with originally cuboid cells (figure 3*a*) deforms, such that the initially vertical walls bend into circular walls, while the horizontal walls remain virtually horizontal and may contract longitudinally (figure 3*b*,*c*). When the cells are filled with a compliant liquid or solid core, and the internal volume of the cells is preserved throughout the deformation, pre-stretching of the cell walls may be caused by the pressure in the cell core before the walls bend. In order to study the changes in the mechanical properties of the walls in a filled cell compared to those of an empty cell, we assume that in both cases, the walls are deformed by (2.1) followed by (2.2). *However, the non-zero pressure causing the pre-stretch is maintained in the filled cell, whereas in the empty cell, this pressure is removed*. The same approach is employed for the analysis of other deformations in the subsequent sections.

When the walls bend inside the cell, the distance between the ends of the deformed wall in the empty cell can remain equal to the vertical length of the original wall, i.e.

$$Y_0 = r_1\sin\theta_0 < r_1\theta_0 = r_1\frac{AY_0}{\sqrt{a}}.$$

Hence $A>\sqrt{a}/r_1>\sqrt{a}/r$, for all $r\in[r_1,r_2]$. Then, it is reasonable to assume that, in the filled cell, the vertical distance between the ends of the wall will increase farther than in the empty cell, i.e. $\bar{A}>A$, where $\bar{A}$ and A are the constant parameters for the deformation (2.2) in the filled and the empty cell, respectively (figure 2).

For the deformed state due to (2.2) superposed on (2.1), the radial direction is a principal direction (appendix Aa). Thus, assuming that the resulting deformation is a contraction in the radial direction, i.e. $B_{rr}=a^2/r^2<1$, by the PC inequalities, the associated stress component is

negative (radial compression). Setting $\sigma_{rr} = -p_0 \le 0$ at the curved surface $r = r_2$, the radial stress takes the form

$$\sigma_{rr} = -p_0 - \int_{r_2}^{r} \frac{\beta_1}{r}\left(\frac{a^2}{r^2} - \frac{A^2 r^2}{a}\right) \mathrm{d}r + \int_{r_2}^{r} \frac{\beta_{-1}}{r}\left(\frac{a}{A^2 r^2} - \frac{r^2}{a^2}\right) \mathrm{d}r$$
$$\le -p_0, \quad r \in [r_1, r_2].$$

In order to analyse the elasticity of the deformed wall, we define the nonlinear elastic modulus as the ratio between the Cauchy (true) stress and the logarithmic (true) strain (the sum of all the small strain increments) in the radial direction

$$\mathcal{E} = \frac{\sigma_{rr}}{\ln B_{rr}^{1/2}}. \tag{2.3}$$

We first compare the values of the modulus of elasticity (2.3) when the cell is empty and when the cell is filled with an incompressible fluid or solid core. Let $\bar{\boldsymbol{\sigma}}$ and $\boldsymbol{\sigma}$ represent the Cauchy stress of the wall in a filled and an empty cell, respectively, and $\bar{\mathcal{E}}$ and $\mathcal{E}$ denote the corresponding elastic moduli. If $\bar{\sigma}_{rr}(r_2) = -p_0 < 0$ and $\sigma_{rr}(r_2) = 0$, then, at equal strains

$$\bar{\mathcal{E}} - \mathcal{E} = -\frac{p_0}{\ln(a/r)} + \frac{1}{\ln(a/r)} \int_{r_2}^{r} \frac{\beta_1 r}{a}(\bar{A}^2 - A^2)\, \mathrm{d}r + \frac{1}{\ln(a/r)} \int_{r_2}^{r} \frac{\beta_{-1} a}{r^3}\left(\frac{1}{\bar{A}^2} - \frac{1}{A^2}\right) \mathrm{d}r$$
$$\ge -\frac{p_0}{\ln(a/r)} > 0, \quad r \in [r_1, r_2].$$

Hence the radial elastic modulus of the deformed wall is larger in the filled cell than in the empty cell, and the gap between the respective moduli increases as the magnitude of $-p_0$ increases.

Another interesting situation is when the internal volume of the filled cell begins to increase under the combined deformations (2.1) and (2.2) of the cell walls, and the walls become free from the pressure due to the incompressible inclusion, which now occupies less than the total internal volume of the deformed cell. In this cell, the vertical distance between the ends of the wall may increase farther than in the filled cell with fixed internal volume, and we set $\bar{\bar{A}} = \sqrt{\bar{A}^2 + \delta^2}$ as the constant parameter for the deformation (2.2), where $\delta^2 > 0$.

Let $\bar{\boldsymbol{\sigma}}$ and $\bar{\bar{\boldsymbol{\sigma}}}$ denote the Cauchy stress of the wall in a filled cell with fixed and increased internal volume, respectively, and $\bar{\mathcal{E}}$ and $\bar{\bar{\mathcal{E}}}$ be the respective elastic moduli. If $\bar{\sigma}_{rr}(r_2) = -p_0 < 0$ and $\bar{\bar{\sigma}}_{rr}(r_2) = 0$, then, at equal strains

$$\bar{\mathcal{E}} - \bar{\bar{\mathcal{E}}} = -\frac{p_0}{\ln(a/r)} - \frac{\delta^2}{\ln(a/r)} \int_{r_2}^{r} \frac{\beta_1 r}{a}\, \mathrm{d}r + \frac{\delta^2}{\bar{A}^2(\bar{A}^2 + \delta^2)\ln(ar)} \int_{r_2}^{r} \frac{\beta_{-1} a}{r^3}\, \mathrm{d}r,$$
$$\le -\frac{p_0}{\ln(a/r)} > 0, \quad r \in [r_1, r_2],$$

and there exists $\delta_0^2 > 0$, such that

$$\bar{\mathcal{E}} - \bar{\bar{\mathcal{E}}} > 0, \quad \forall\, \delta^2 \in (0, \delta_0^2).$$

This situation is possible, for example, when gaps begin to appear between the cell walls and the cell core, rendering the walls virtually free from the original internal pressure.

Finally, comparing the elastic moduli in the cell with increasing internal volume and in the empty cell, we obtain

$$\bar{\bar{\mathcal{E}}} - \mathcal{E} = \frac{1}{\ln(a/r)} \int_{r_2}^{r} \frac{\beta_1 r}{a}(\bar{\bar{A}}^2 - A^2)\, \mathrm{d}r + \frac{1}{\ln(a/r)} \int_{r_2}^{r} \frac{\beta_{-1} a}{r^3}\left(\frac{1}{\bar{\bar{A}}^2} - \frac{1}{A^2}\right) \mathrm{d}r$$
$$> 0, \quad r \in [r_1, r_2].$$

We conclude that

$$\bar{\mathcal{E}} > \bar{\bar{\mathcal{E}}} > \mathcal{E},$$

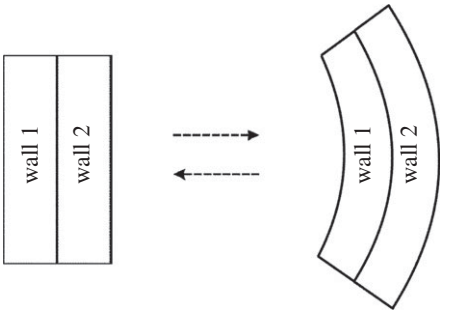

Figure 4. Schematic of elastic bending of two-layer wall.

i.e. the radial elastic modulus of the deforming wall is larger in the filled cell with fixed internal volume (and non-zero cell pressure) than when the internal volume increases (and there is no internal pressure), and smaller in the empty cell.

Next, we compare the behaviour of two walls of different thickness subject to the successive deformations (2.1) and (2.2). Taking the original wall as the 'thin' wall, we assume that the 'thicker' wall occupies the reference domain $[C_1, C_2'] \times [-Y_0, Y_0] \times [-Z_0, Z_0]$, where $C_2' > C_2$, and denote by $\boldsymbol{\sigma}'$ the Cauchy stress in this wall, and by $\mathcal{E}'$ the associated elastic modulus (2.3). Then setting $\sigma_{rr}'(r_2') = \sigma_{rr}(r_2) = -p_0 \le 0$, at equal strains, we obtain

$$\begin{aligned}\mathcal{E}' - \mathcal{E} &= -\frac{1}{\ln(a/r)} \int_{r_2'}^{r_2} \frac{\beta_1}{r} \left(\frac{a^2}{r^2} - \frac{A^2 r^2}{a} \right) \mathrm{d}r + \frac{1}{\ln(a/r)} \int_{r_2'}^{r_2} \frac{\beta_{-1}}{r} \left(\frac{a}{A^2 r^2} - \frac{r^2}{a^2} \right) \mathrm{d}r \\ &> 0, \quad r \in [r_1, r_2].\end{aligned}$$

Hence the radial elastic modulus increases as the thickness of the cell wall increases.

We further consider the case when a second wall is 'attached' to the first wall in the sense that the relative radial displacement across the common interface is equal to zero, and both walls deform by the successive deformations (2.1) and (2.2). Specifically, let the second wall occupy the domain $[C_2, C_2'] \times [-Y_0, Y_0] \times [-Z_0, Z_0]$ in the reference state, and $[r_2, r_2'] \times [-\theta_0, \theta_0] \times [-z_0, z_0]$ in the deformed state, where $C_2' > 0$ and $r_2' > 0$ are constants (figure 4).

We wish to verify how the stiffness of the first wall is modified by the presence of the second wall. We denote by $\boldsymbol{\sigma}'$ the Cauchy stress for either walls, and by $\mathcal{E}'$ the associated radial elastic modulus (2.3). When the radial strain satisfies $B_{rr} < 1$ for both walls, setting $\sigma_{rr}'(r_2') = -p_0 \le 0$, the radial stress of the second wall takes the form

$$\sigma_{rr}'(r) = -p_0 - \int_{r_2'}^{r} \frac{\beta_1'}{r} \left(\frac{a^2}{r^2} - \frac{A^2 r^2}{a} \right) \mathrm{d}r + \int_{r_2'}^{r} \frac{\beta_{-1}'}{r} \left(\frac{a}{A^2 r^2} - \frac{r^2}{a^2} \right) \mathrm{d}r \le -p_0, \quad r \in [r_2, r_2'],$$

where $\beta_1' > 0$, $\beta_{-1}' \le 0$ are the material responses for this wall.

For the first wall, the radial stress is

$$\begin{aligned}\sigma_{rr}'(r) &= \sigma_{rr}'(r_2) - \int_{r_2}^{r} \frac{\beta_1}{r} \left(\frac{a^2}{r^2} - \frac{A^2 r^2}{a} \right) \mathrm{d}r + \int_{r_2}^{r} \frac{\beta_{-1}}{r} \left(\frac{a}{A^2 r^2} - \frac{r^2}{a^2} \right) \mathrm{d}r \\ &\le \sigma_{rr}'(r_2), \quad r \in [r_1, r_2],\end{aligned}$$

where $\beta_1 > 0$, $\beta_{-1} \le 0$ are the corresponding material responses.

If $\boldsymbol{\sigma}$ represents the Cauchy stress of the original wall when no other wall is attached, such that $\sigma_{rr}(r_2) = -p_0$, then, at the same strain

$$\begin{aligned}\mathcal{E}' - \mathcal{E} = \frac{\sigma_{rr}'(r_2) + p_0}{\ln B_{rr}^{1/2}} &= -\frac{1}{\ln(a/r)} \int_{r_2'}^{r_2} \frac{\beta_1'}{r} \left(\frac{a^2}{r^2} - \frac{A^2 r^2}{a} \right) \mathrm{d}r + \frac{1}{\ln(a/r)} \int_{r_2'}^{r_2} \frac{\beta_{-1}'}{r} \left(\frac{a}{A^2 r^2} - \frac{r^2}{a^2} \right) \mathrm{d}r \\ &> 0, \quad r \in [r_1, r_2].\end{aligned}$$

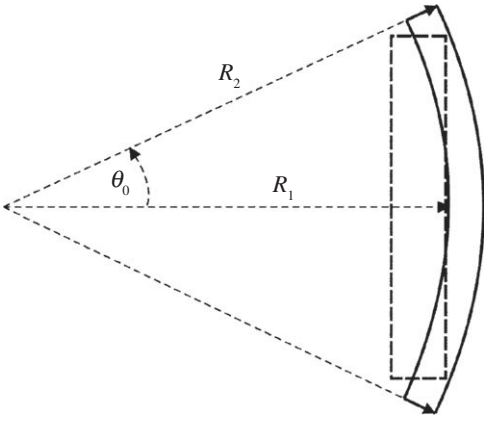

Figure 5. Schematic of straightening of a curved wall.

Hence the radial elastic modulus of the first wall is larger when a second wall is attached to it in the direction of its decreasing curvature. Since the magnitude of $\sigma'_{rr}(r_2)$ relative to $-p_0$ increases when the thickness of the second wall increases, the elastic modulus of the first wall increases with the thickness of the attached wall.

This analysis extends directly to the case of multi-layer cell walls. In particular, when a third wall with the reference domain $[C'_2, C''_2] \times [-Y_0, Y_0] \times [-Z_0, Z_0]$, where $C''_2 > 0$ is constant, is further attached to the second wall in the direction of its decreasing curvature, and the three walls deform together by (2.2) superposed on (2.1), then the stiffness of both the first and the second (middle) wall is enhanced by the contact with the adjacent walls.

For sandwich structures in bending, the above result implies that the stiffness of the middle layer is enhanced in part by the contact conditions with the adjacent layers.

Similar results are obtained when the wall bends outside the cell, by taking $B_{rr} > 1$ (radial extension). In this case, the vertical distance between the ends of the initially straight wall decreases less for the filled cell than for the empty cell.

(b) Curved walls

A cell wall in the shape of an annular wedge with the reference geometry described by $(R, \Theta, Z) \in [R_1, R_2] \times [-\Theta_0, \Theta_0] \times [-Z_0, Z_0]$, where R_1, R_2, Θ_0 and Z_0 are positive constants, is first deformed by the uniform stretch

$$\tilde{R} = \sqrt{a}R, \quad \tilde{\Theta} = \Theta \quad \text{and} \quad \tilde{Z} = \frac{Z}{a}, \tag{2.4}$$

where $(\tilde{R}, \tilde{\Theta}, \tilde{Z})$ and (R, Θ, Z) are the cylindrical polar coordinates for the deformed and the reference configuration, respectively, and a is a positive constant. For this deformation, the non-zero components of the Cauchy stress tensor are $\sigma^{(0)}_{\tilde{R}\tilde{R}} = \sigma^{(0)}_{\tilde{\Theta}\tilde{\Theta}} = -p_0$ (appendix Ab). In the linear elastic limit, where $a \to 1$, $p_0 = 0$.

Then the deformed wall is 'straightened' into a rectangular block by the deformation:

$$x = \frac{A^2}{2}\tilde{R}^2, \quad y = \frac{\tilde{\Theta}}{A} \quad \text{and} \quad z = \frac{\tilde{Z}}{A}, \tag{2.5}$$

where $(x, y, z) \in [c_1, c_2] \times [-y_0, y_0] \times [-z_0, z_0]$ are the Cartesian coordinates for the current configuration, and c_1, c_2, y_0, z_0 and A are positive constants (figure 5).

Assuming that the deformation (2.5) superposed on (2.4) is a contraction in the x-direction, i.e. $B_{xx} = 2A^2 a x < 1$, by the PC inequalities, the associated stress component is compressive

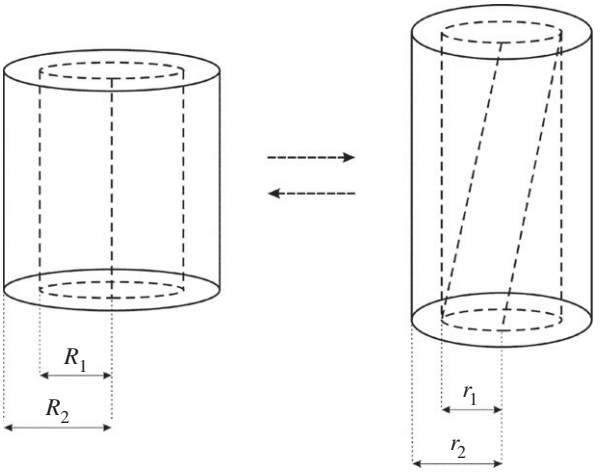

Figure 6. Schematic of combined stretch and torsion of a circular cylindrical tube.

(appendix A*b*)

$$\sigma_{xx} = -p_0 \le 0, \quad x \in [c_1, c_2].$$

We define the nonlinear elastic modulus as the ratio between the Cauchy stress and the logarithmic strain in the x-direction, as follows:

$$\mathcal{E} = \frac{\sigma_{xx}}{\ln B_{xx}^{1/2}}. \tag{2.6}$$

We compare the values of the modulus of elasticity (2.6) when the cell is empty and when the cell is filled with an incompressible core. Let $\bar{\boldsymbol{\sigma}}$ and $\boldsymbol{\sigma}$ denote the Cauchy stress for the filled cell and the empty cell, respectively, and $\bar{\mathcal{E}}$ and $\mathcal{E}$ be the corresponding elastic moduli. Setting $\bar{\sigma}_{xx} = -p_0 < 0$ and $\sigma_{xx} = 0$, we obtain

$$\bar{\mathcal{E}} - \mathcal{E} = -\frac{p_0}{\ln(A\sqrt{2ax})} > 0, \quad x \in [c_1, c_2],$$

i.e. the elastic modulus in the transverse direction of the deformed wall is greater in the filled cell than in the empty cell, and the gap between the two moduli increases as the magnitude of $-p_0$ increases.

As σ_{xx} is constant, if $-p_0 < 0$, then the elastic modulus (2.6) is an increasing function of x, and this modulus increases as the thickness of the wall increases.

Analogous results are obtained when $B_{xx} > 1$.

(c) Circular tubes

A circular cylindrical tube which occupies the domain $(R, \Theta, Z) \in [R_1, R_2] \times [-\Theta_0, \Theta_0] \times [-Z_0, Z_0]$ in the undeformed (reference) configuration, where R_1, R_2, Θ_0 and Z_0 are positive constants, is first deformed by the uniform stretch (2.4). The deformed tube is then further subjected to the simple torsion

$$r = \tilde{R}, \quad \theta = \tilde{\Theta} + \tau\tilde{Z} \quad \text{and} \quad z = \tilde{Z}, \tag{2.7}$$

where (r, θ, z) and $(\tilde{R}, \tilde{\Theta}, \tilde{Z})$ are the cylindrical polar coordinates for the current and the pre-deformed tube, respectively, and τ is a positive constant (figure 6).

For the current state, due to the successive deformations (2.4) and (2.7), the radial direction is a principal direction (appendix Ac). Thus, assuming that the resulting deformation is a contraction

in the radial direction, i.e. $B_{rr} = a < 1$, by the PC inequalities, the associated stress component is negative (radial compression). Setting $\sigma_{rr} = -p_0 \leq 0$ at the external surface $r = r_2$, we obtain

$$\sigma_{rr} = -p_0 + \int_{r_2}^{r} \beta_1 r \frac{\tau^2}{a^2}\, \mathrm{d}r \leq 0, \quad r \in [r_1, r_2].$$

We define the nonlinear elastic modulus as the ratio between the Cauchy stress and the logarithmic strain in the radial direction, as follows:

$$\mathcal{E} = \frac{\sigma_{rr}}{\ln B_{rr}^{1/2}}. \tag{2.8}$$

We first compare the values of the modulus of elasticity (2.8) when the tube is empty and when the tube is filled with an incompressible core. Let $\bar{\boldsymbol{\sigma}}$ and $\boldsymbol{\sigma}$ denote the Cauchy stress for the filled tube and the empty tube, respectively, and $\bar{\mathcal{E}}$ and $\mathcal{E}$ be the corresponding elastic moduli. Setting $\bar{\sigma}_{rr}(r_2) = -p_0 < 0$ and $\sigma_{rr}(r_2) = 0$, at equal strains, we deduce that

$$\bar{\mathcal{E}} - \mathcal{E} = -\frac{p_0}{\ln \sqrt{a}} > 0, \quad r \in [r_1, r_2].$$

Hence the radial elastic modulus of the deformed wall is greater for the filled tube than for the empty tube, and the gap between the respective moduli increases as the magnitude of $-p_0$ increases.

Next, we compare the behaviour of two tubes with different wall thickness. Let $\boldsymbol{\sigma}'$ denote the Cauchy stress when $r_2' > r_2$ and $r_1' = r_1$, and $\mathcal{E}'$ be the associated elastic modulus (2.8). Since σ_{rr} is an increasing function of r, if $\sigma_{rr}'(r_2') = \sigma_{rr}(r_2) = -p_0 \leq 0$, then

$$\mathcal{E}' - \mathcal{E} = \frac{1}{\ln \sqrt{a}} \int_{r_2'}^{r_2} \beta_1 r \frac{\tau^2}{a^2}\, \mathrm{d}r > 0, \quad r \in [r_1, r_2],$$

i.e. the elastic modulus in the radial direction increases when the thickness of the tube wall increases.

We also examine the case when the original tube is surrounded by a second tube which is 'attached' to it in the sense that the relative radial displacement across the common interface is equal to zero, and both tubes deform by the successive deformations (2.4) and (2.7). Specifically, when the second tube occupies the domain $[R_2, R_2'] \times [-\Theta_0, \Theta_0] \times [-Z_0, Z_0]$ in the reference configuration, and $[r_2, r_2'] \times [-\theta_0, \theta_0] \times [-z_0, z_0]$ in the deformed configuration, where $R_2' > 0$ and $r_2' > 0$ are constants, we wish to verify how the stiffness of the first tube is modified by the presence of the surrounding tube.

We denote by $\boldsymbol{\sigma}'$ the Cauchy stress for either tubes, and by $\mathcal{E}'$ the associated elastic modulus (2.8). If the radial strain satisfies $B_{rr} < 1$ for both tubes, then setting $\sigma_{rr}'(r_2') = -p_0 \leq 0$, the radial stress of the second tube takes the form

$$\sigma_{rr}'(r) = -p_0 + \int_{r_2'}^{r} \beta_1' r \frac{\tau'^2}{a^2}\, \mathrm{d}r \leq 0 \leq -p_0, \quad r \in [r_2, r_2'],$$

where $\beta_1' > 0$ is the material response for this tube and $\tau' > 0$.

For the first tube, the radial stress is

$$\sigma_{rr}' = \sigma_{rr}'(r_2) + \int_{r_2}^{r} \beta_1 r \frac{\tau^2}{a^2}\, \mathrm{d}r \leq \sigma_{rr}'(r_2), \quad r \in [r_1, r_2],$$

where $\beta_1 > 0$ is the corresponding material response and $\tau > 0$.

At the same strain, if $\boldsymbol{\sigma}$ represents the Cauchy stress of the original wall when no other wall is attached, such that $\sigma_{rr}(r_2) = -p_0$, then

$$\begin{aligned}\mathcal{E}' - \mathcal{E} &= \frac{\sigma_{rr}'(r_2) + p_0}{\ln B_{rr}^{1/2}} \\ &= \frac{1}{\ln \sqrt{a}} \int_{r_2'}^{r_2} \beta_1' r \frac{\tau'^2}{a^2}\, \mathrm{d}r > 0, \quad r \in [r_1, r_2].\end{aligned}$$

Hence the radial elastic modulus in the first tube is greater when it is surrounded by a second tube. As the magnitude of $\sigma'_{rr}(r_2)$ relative to $-p_0$ increases as the thickness of the second tube increases, the elastic modulus of the first tube also increases when the thickness of the surrounding tube increases.

The extension to the case of multiple tubes is then straightforward. For example, when the second tube is further surrounded by a third tube with the reference domain $[R'_2, R''_2] \times [-\Theta_0, \Theta_0] \times [-Z_0, Z_0]$, where $R''_2 > 0$ is constant, and all three tubes deform simultaneously by (2.7) superposed on (2.4), then the stiffness of both the first and the second (middle) tube is enhanced by the contact with their surrounding tubes.

Another result of interest concerns the changes in the mechanical properties of a solid elastic core which occupies the interior of a filled circular tube when subject to combined stretch and torsion. This corresponds to the case when a circular tube is filled with a compliant cylindrical core made from a softer elastic material. The cylinder occupies the domain $[0, R_1] \times [-\Theta_0, \Theta_0] \times [-Z_0, Z_0]$ in the undeformed state, and the tube and the cylinder are deformed simultaneously by the uniform stretch (2.4) followed by the simple torsion (2.7). For the solid cylinder, such that $\sigma_{rr} = -p_0 \leq 0$ at the side surface $r = r_1$, the radial stress satisfies

$$\sigma_{rr} = -p_0 + \int_{r_1}^{r} \beta_1 r \frac{\tau^2}{a^2}\, \mathrm{d}r \leq 0, \quad r \in [0, r_1].$$

We now compare the values of the modulus of elasticity, also defined by (2.8), when the cylinder is free and when it is surrounded by a circular tube. Let $\bar{\boldsymbol{\sigma}}$ and $\boldsymbol{\sigma}$ denote the Cauchy stress of the cylinder when this is enclosed in a tube and when it is free, respectively, and $\bar{\mathcal{E}}$ and $\mathcal{E}$ be the corresponding elastic moduli. Since $B_{rr} < 1$, at equal strains, setting $\bar{\sigma}_{rr}(r_1) = -p_0 < 0$ and $\sigma_{rr}(r_1) = 0$, we obtain

$$\bar{\mathcal{E}} - \mathcal{E} = -\frac{p_0}{\ln \sqrt{a}} > 0, \quad r \in [0, r_1].$$

Hence the radial elastic modulus is greater for the cylinder deforming within the tube, and the gap between the moduli increases as the magnitude of $-p_0$ increases.

For two cylinders of different initial radius, let $\boldsymbol{\sigma}'$ be the radial stress when $r'_1 > r_1$, and $\mathcal{E}'$ be the associated elastic modulus (2.8). Setting $\sigma'_{rr}(r'_1) = \sigma_{rr}(r_1) = -p_0 \leq 0$ implies

$$\mathcal{E}' - \mathcal{E} = \frac{1}{\ln \sqrt{a}} \int_{r'_1}^{r_1} \beta_1 r \frac{\tau^2}{a^2}\, \mathrm{d}r > 0, \quad r \in [0, r_1],$$

i.e. the elastic modulus in the radial direction increases as the radius of the cylinder increases.

The results of this section, for three different non-homogeneous deformations, namely the bending of a rectangular wall, the straightening of a curved wall, and the torsion of circular tube, uncover some of the generic elastic properties underpinning the mechanical performance of cellular structures of nonlinear elastic material at individual cell level, such as *the increase in the elastic modulus of a cell wall with the wall thickness and the cell pressure*. By a similar approach, we also find that, *for sandwich structures in bending, the middle layer becomes stiffer due to the contact conditions with the adjacent layers*, and similarly, *the soft elastic core of a circular tube becomes stiffer when deformed with the tube*. Since the (constrained or unconstrained) deformations analysed here can be maintained in every homogeneous, incompressible, isotropic, hyperelastic material, our results are independent of the strain energy function describing the cell-wall material.

3. Numerical examples

In order to examine how the elasticity of the cell walls is affected by the presence of compliant inclusions in an assembly of cells deforming together under the influence of external forces, computational models are required. In this section, the constant parameters, although within a realistic range [27], are purely for numerical exemplification, and do not correspond to actual

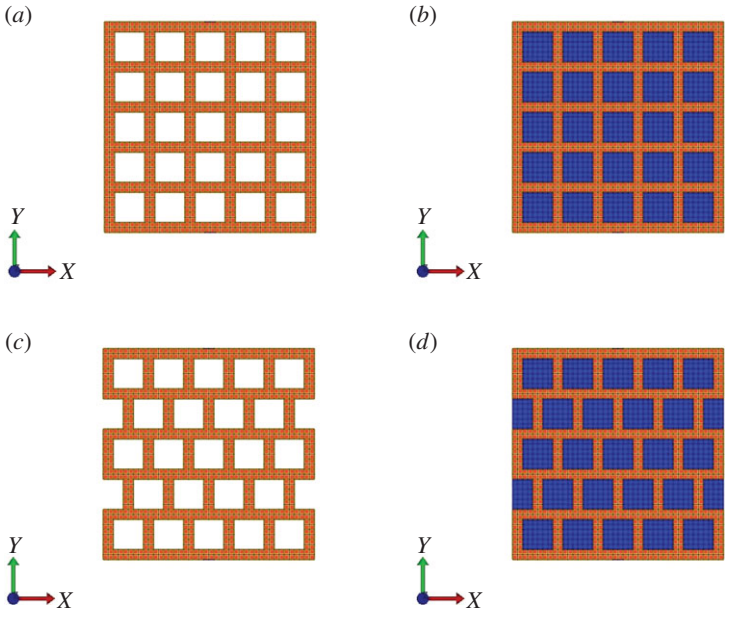

Figure 7. Undeformed (*a*,*c*) honeycomb structures and (*b*,*d*) cellular pads with (*a*,*b*) stacked and (*c*,*d*) staggered cells. (Online version in colour.)

data. However, it is hoped that our results may generate further interest in this topic, including further experimental testing of natural cellular pads.

The numerical results reported here were obtained by a standard finite-element procedure implemented within the open-source software Finite Elements for Biomechanics (FEBio) environment [28]. The cellular structures in figure 7*a*,*c* are made from a single piece of elastic material which occupies a thin square domain of (dimensionless) side one in the X-(horizontal) and Y-(vertical) directions. The cells are squares of approximate side 0.2 in the horizontal and vertical directions, and are arranged periodically in a stacked or staggered configuration throughout the structure. The cellular pads in figure 7*b*,*d* are obtained by filling the empty cells of the corresponding honeycomb structure with a hyperelastic material which is 10 or 20 times softer than the cell-wall material, and complies with the deformation of the cell walls in the sense that the displacements are continuous across the interface between the walls and the inclusions. In these figures, the finite-element mesh is also shown. For the underlying structural materials, we choose two different hyperelastic models.

Neo-Hookean (NH): In the first model, the cell walls and the cell cores are characterized by a compressible NR strain-energy function of the form

$$\mathcal{W}(I_1, I_2, I_3) = \frac{\mu}{2}\left(I_3^{-1/3} I_1 - 3 - \ln I_3\right) + \frac{\lambda}{2}\left(\ln I_3^{1/2}\right)^2, \tag{3.1}$$

where $\mu = E/2(1+\nu)$ and $\lambda = \nu E/(1+\nu)(1-2\nu)$ are constant material parameters. In the numerical examples, we set $E = 0.1$ MPa and $\nu = 0.49$ for the cell walls, and $E = 0.01$ MPa (cellular pads 1) or $E = 0.005$ MPa (cellular pads 2) and $\nu = 0.495$ for the cell cores.

Mooney–Rivlin (MR): In the second model, the elastic materials in the cell walls and the cell inclusions are described by the generalized MR strain-energy density

$$\mathcal{W}(I_1, I_2, I_3) = \frac{\mu_1}{2}\left(I_3^{-1/3} I_1 - 3\right) + \frac{\mu_2}{2}\left(I_3^{-2/3} I_2 - 3\right) + \frac{\kappa}{2}\left(I_3^{1/2} - 1\right)^2, \tag{3.2}$$

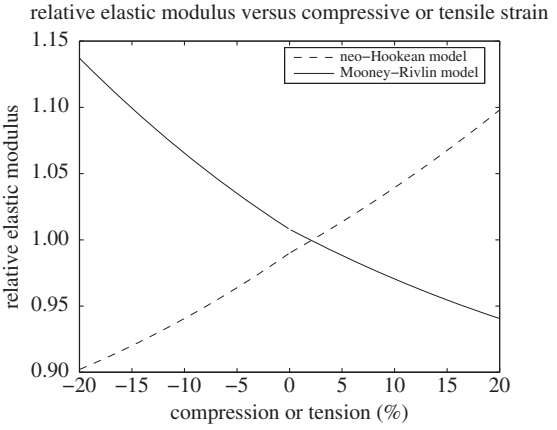

Figure 8. Nonlinear elastic modulus $\mathcal{E}$ normalized to E for the NH and MR models.

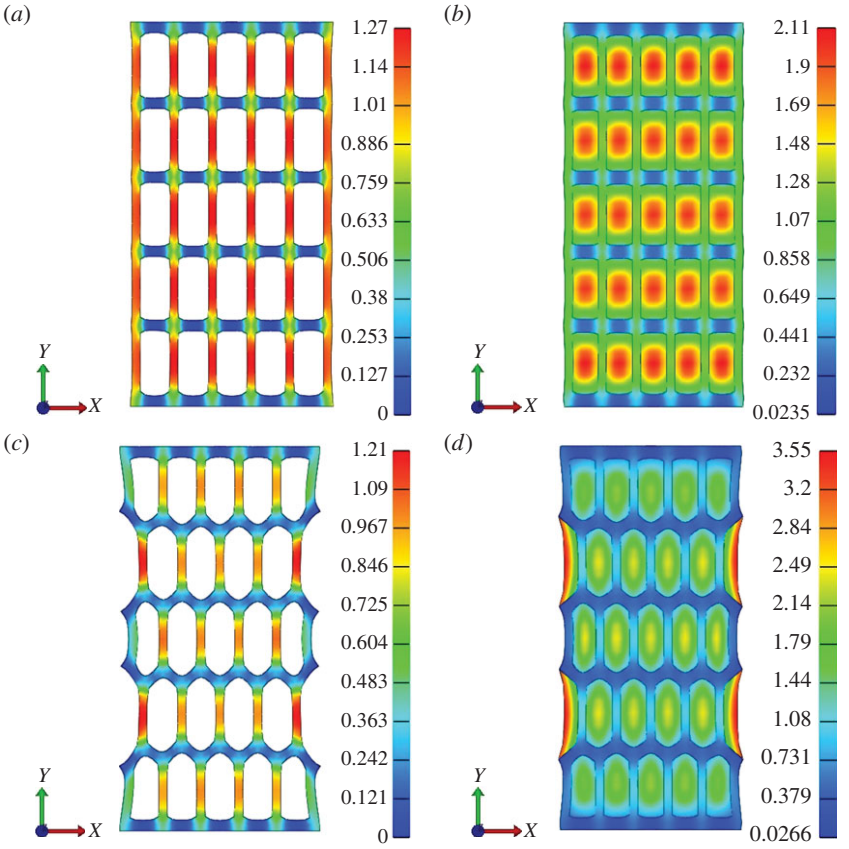

Figure 9. Deformed structures with NH components under prescribed vertical stretch of 75% at the top external boundary, showing the Green-Lagrange strain in the vertical direction for (*a*,*c*) honeycomb structures and (*b*,*d*) cellular pads 1 with (*a*,*b*) stacked and (*c*,*d*) staggered cells. (Online version in colour.)

where μ_1, μ_2, κ are constants, such that $\mu = \mu_1 + \mu_2 > 0$ and $\kappa > 0$. In the numerical models, we set $\mu_1 = 0.0016$ MPa, $\mu_2 = 0.032$ MPa, $\kappa = 1.6667$ MPa for the cell walls, and $\mu_1 = 0.0001$ MPa, $\mu_2 = 0.0032$ MPa, $\kappa = 0.3333$ MPa (cellular pads 1) or $\mu_1 = 0.0002$ MPa, $\mu_2 = 0.0015$ MPa, $\kappa = 0.1667$ MPa (cellular pads 2) for the inclusions.

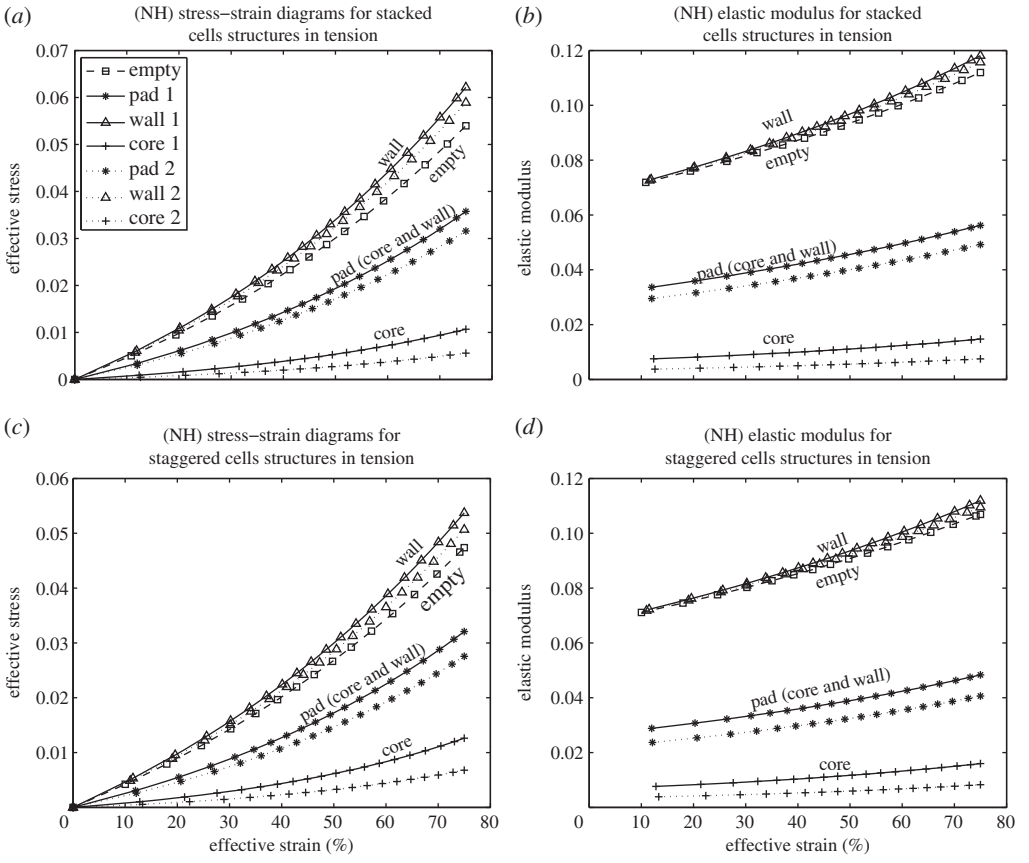

Figure 10. (*a*,*c*) Mean effective Cauchy stress (MPa) and (*b*,*d*) apparent elastic modulus (MPa) versus mean effective logarithmic strain for cellular structures with (*a*,*b*) stacked and (*c*,*d*) staggered cells of NH material.

These models are suitable representatives of nonlinear hyperelastic materials exhibiting different mechanical behaviours under simple tension or compression. Specifically, if the elastic modulus is defined by

$$\mathcal{E} = \frac{a^3 - 1}{a \ln a}\left(\beta_1 - \frac{\beta_{-1}}{a}\right), \tag{3.3}$$

where $a > 0$ is the stretch in the direction of the applied tensile or compressive force, then for the NH model (3.1), this modulus increases as tension increases and decreases as compression increases, while for the MR model (3.2), the elastic modulus (3.3) decreases under increasing tension and increases under increasing compression (figure 8). *The question is how the material properties of the walls and core affect the mechanical behaviour of the cellular structure?*

The model structures are subjected to vertical tension, where the conditions at the external boundaries are as follows: the lower external horizontal face is free to slide in the first/horizontal/X-direction and is fixed in the second/vertical/Y-direction and also in the third/out-of-plane/Z-direction, the upper external horizontal face is subject to a prescribed vertical stretch of 75%, and is free to slide horizontally and fixed in the Z-direction, while all the other external faces deform freely. For the honeycombs, the internal cell faces are free, while for the cellular pads, the displacements are continuous across the interface between the cell walls and cell cores. The deformation of the cellular structures of NH materials where $E = 0.1$ MPa for the cell walls and $E = 0.01$ MPa for the cell cores are depicted in figure 9. Note that, for the structures with staggered cells, the original horizontal walls appear to 'bend' outside the cells. Analogous deformations were observed in structures made from MR materials.

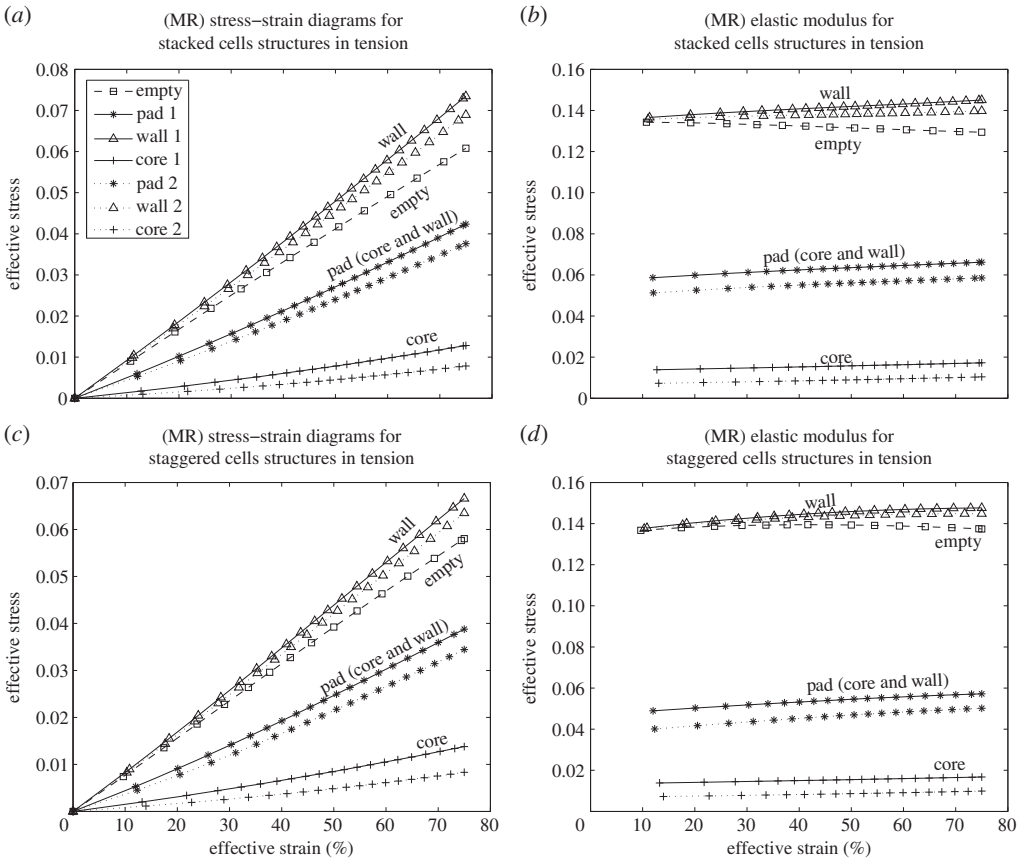

Figure 11. (*a*,*c*) Mean effective Cauchy stress (MPa) and (*b*,*d*) apparent elastic modulus (MPa) versus mean effective logarithmic strain for cellular structures with (*a*,*b*) stacked and (*c*,*d*) staggered cells of MR material.

In figures 10*a*,*c* and 11*a*,*c*, we record the average values of the effective Cauchy stress versus those of the effective logarithmic strain throughout the solid matter. In figures 10*b*,*d* and 11*b*,*d*, the *apparent elastic modulus* representing the ratio between the mean effective Cauchy stress and the mean effective logarithmic strain is indicated. From these results, we infer that the cell walls are stiffer in the cellular pads than in the corresponding honeycombs, and also in structures where the elastic modulus of the inclusions is higher (cellular pads 1) compared with those where the elastic modulus of the inclusions is lower (cellular pads 2). The numerical results for the staggered cells in figures 10 and 11 differ only slightly from those corresponding to the stacked cells, suggesting that the observed behaviour is mainly due to the elastic stretch, while the bending of the initially horizontal walls in the staggered cells is responsible for a reduction in both the stress level and the stiffness of the cell walls relative to those in the stacked cells.

In the plots, square symbols correspond to the cell walls in the empty cells structure, stars are for the overall filled cells structure (cellular pad), triangles correspond to the cell walls in the cellular pad, and plus symbols are for the cell cores. An average value is computed by summing the associated values on all the finite elements and dividing by the number of elements.

For structures made from NH and MR components (figures 10 and 11 respectively), as the deformation increases, the elastic modulus in the cell walls of NH material increases whereas in those made from MR material decreases, but in all cases the stiffness of the cell inclusions increases. Consequently, while the mean elastic modulus of the cellular pads made from NH materials clearly increases, the modulus of the pads made from MR materials is almost constant. This is an interesting result which suggests that soft cellular pads with an elastic

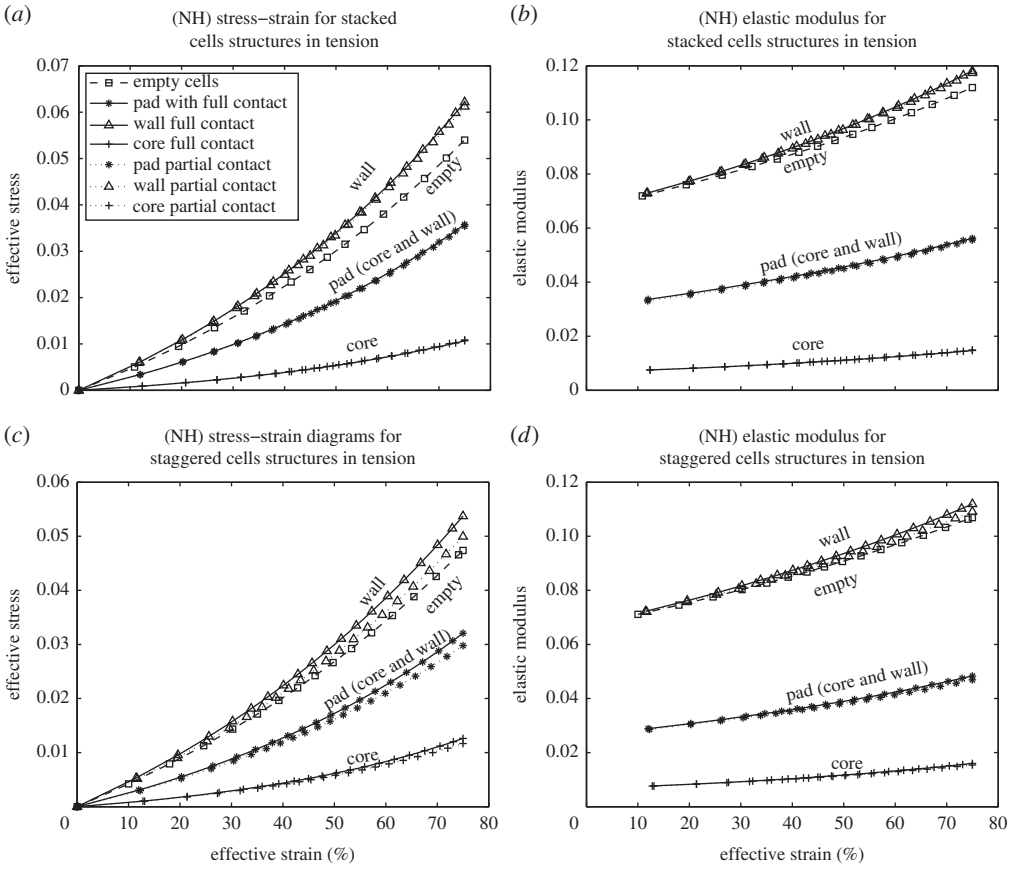

Figure 12. (*a*,*c*) Mean effective Cauchy stress (MPa) and (*b*,*d*) apparent elastic modulus (MPa) versus mean effective logarithmic strain for cellular structures of NH material with different contact conditions between cell walls and cell cores.

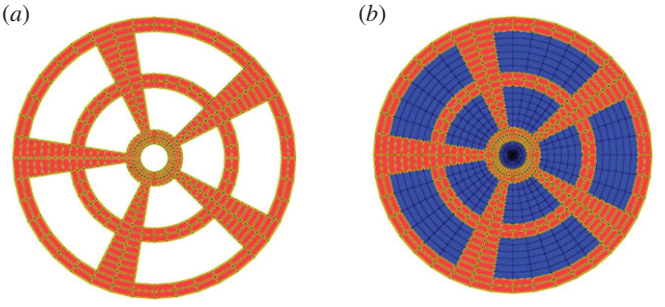

Figure 13. Cross section of undeformed (*a*) cylindrical structure and (*b*) cellular pad with wedge-shaped cells. (Online version in colour.)

modulus that remains almost constant may be designed from nonlinear elastic components. The mechanism responsible for this phenomenon deserves further consideration and will be studied separately elsewhere.

We further assess the apparent elastic modulus of cellular pads when gaps are allowed to open between vertical walls and cell cores. In this case, figure 12 shows that the stiffness of the cell walls, although still higher than in the empty cells, is lower than when contact between cell walls and cell cores is maintained everywhere.

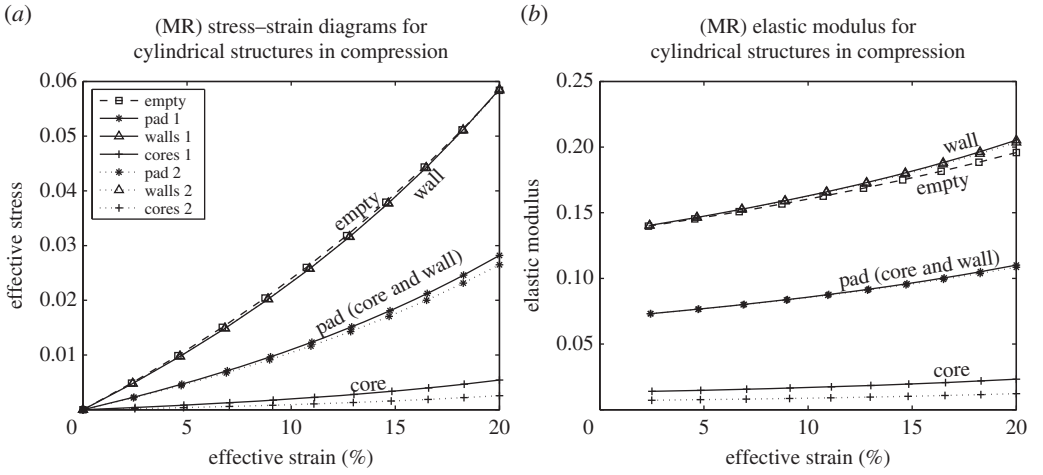

Figure 14. (*a*) Mean effective Cauchy stress (MPa) and (*b*) apparent elastic modulus (MPa) versus mean effective logarithmic strain for cylindrical cellular structures with wedge shaped cells of MR material.

Finally, we model cylindrical structures with wedge-shaped cells which are either empty or filled with compliant cores. For these models, the radius of the cross section is (dimensionless) unity, the height is 0.2, and the cross-section geometry is illustrated in figure 13. The corresponding boundary conditions are a small twist (1.5%) superposed on axial compression (up to 20%) prescribed on the upper circular face, zero displacements on the lower circular face and free side surface, while the internal faces of the empty cells are free, and at the interface between the cell walls and the cell cores, the displacements are continuous. For structures made from MR materials, the resulting stress–strain diagrams and elastic moduli are indicated in figure 14. In this case also, the apparent elastic modulus of the cell walls is larger when the cells are filled than when the cells are empty, and also when the elastic modulus of the elastic core is higher (cylindrical pad 1) than when the elastic modulus of the core is lower (cylindrical pad 2).

In summary, for model structures made from different hyperelastic materials, our numerical results show that the apparent elastic modulus of the cell walls in the direction of the applied force is greater when the cells are filled with an elastic core than when the cells are empty, and increases as the pressure in the cell core increases. This is in agreement with the analytical results of the previous section, where the deformations were pre-defined, and may be regarded as an extension of those results to the more general deformations of these structures.

4. Conclusion

Paws, plantar pads and plant stems are some of the most remarkable load-bearing biological structures. They generally rely on closed cells filled with fluids or adipose tissue to cushion large distortions. During deformation, the key quantity to characterize the response of such structures is the *nonlinear elastic modulus*, which we defined as the ratio between stress and strain in a direction associated with the largest change of curvature. We showed for three different geometries that the elastic modulus (i) is greater when the cell is closed and filled with an incompressible liquid or solid core; (ii) increases as the pre-stress due to pressure in the cell core increases; and (iii) increases also when the thickness of the cell wall increases or when the wall is multi-layer. It is important to note that these theoretical results are universal as they do not depend on the specific material model used to describe the cell walls. Therefore, they apply to a wide range of cellular structures made from different isotropic, nonlinear, hyperelastic materials.

For assemblies of cells deforming under external forces, numerical models show that the increase in the elastic modulus of the cell walls with the increasing core pressure is valid throughout the structure. In general, the cell walls are under tension or compression due to the pressure in the cell chamber, and while at low strains also the stiffness of the cell walls was found to be enhanced in part by the presence of incompressible inclusions, *the change in the elastic modulus with the cell pressure is captured only when large strains occur*. In particular, the nonlinear elastic models analysed here offer reasonable characterization of the increase in the elastic moduli of *atrophied heel pads with thicker septa and reduced fat tissue*. Anisotropy of the cell walls likely contributes to further enhance this mechanical behaviour as it allows for a non-monotonous change of thickness during extension [29]. Clearly, these structures are highly hierarchical and rely on a unique micro-mechanical design to create non-trivial macroscopic responses during sustained extreme use. Despite their true biophysical complexity, the fundamental mechanical framework proposed here may be relevant in understanding pathologies or impairments related to the weight bearing and protective ability of heel pads.

Data accessibility. All data for this research are openly available at doi:10.17035/d.2015.100092.

Authors' contributions. L.A.M. and A.G. conceived of and designed the study, carried out the analysis and drafted the manuscript; K.A. carried out the computational work and participated in the numerical analysis. All authors gave final approval for publication.

Competing interests. We declare we have no competing interests.

Funding. A.G. is a Wolfson/Royal Society Merit Award Holder and acknowledges support by the Marie Curie European Reintegration Grant BKRVRG0. K.A. is funded by a scholarship from the Saudi Arabia Government. The support for L.A.M. by the Engineering and Physical Sciences Research Council of Great Britain under research grant EP/M011992/1 is gratefully acknowledged.

Appendix A

(a) Bending of a rectangular wall

For the deformation (2.1), the non-zero components of the corresponding Cauchy stress tensor are as follows:

$$\sigma^{(0)}_{\tilde{X}\tilde{X}} = -p + \beta_1 a^2 + \frac{\beta_{-1}}{a^2} \quad \text{and} \quad \sigma^{(0)}_{\tilde{Y}\tilde{Y}} = \sigma^{(0)}_{\tilde{Z}\tilde{Z}} = -p + \frac{\beta_1}{a} + \beta_{-1} a.$$

After the successive deformations (2.1) and (2.2), the left Cauchy-Green strain tensor, in terms of the current cylindrical polar coordinates (r, θ, z), is equal to

$$\mathbf{B} = \begin{bmatrix} \dfrac{a^2}{r^2} & 0 & 0 \\ 0 & \dfrac{A^2 r^2}{a} & 0 \\ 0 & 0 & \dfrac{1}{(A^2 a)} \end{bmatrix},$$

and the non-zero components of the corresponding Cauchy stress tensor depend only on the radius r [13, p. 187]

$$\sigma_{rr} = -\int \frac{\beta_1}{r}\left(\frac{a^2}{r^2} - \frac{A^2 r^2}{a}\right) \mathrm{d}r + \int \frac{\beta_{-1}}{r}\left(\frac{a}{A^2 r^2} - \frac{r^2}{a^2}\right) \mathrm{d}r,$$

$$\sigma_{\theta\theta} = \sigma_{rr} - \beta_1\left(\frac{a^2}{r^2} - \frac{A^2 r^2}{a}\right) + \beta_{-1}\left(\frac{a}{A^2 r^2} - \frac{r^2}{a^2}\right),$$

$$\sigma_{zz} = \sigma_{rr} + \beta_1\left(\frac{1}{A^2 a} - \frac{a^2}{r^2}\right) - \beta_{-1}\left(\frac{r^2}{a^2} - A^2 a\right).$$

(b) Straightening of an annular wedge

For the deformation (2.4), the non-zero components of the Cauchy stress tensor are [13, p. 190]

$$\sigma^{(0)}_{\tilde{R}\tilde{R}} = \sigma^{(0)}_{\tilde{\Theta}\tilde{\Theta}} = -p_0 \qquad \sigma^{(0)}_{\tilde{Z}\tilde{Z}} = -p_0 - \beta_1 a\left(1 - \frac{1}{a^3}\right) + \frac{\beta_{-1}}{a}(a^3 - 1).$$

After the successive deformations (2.4) and (2.5), the left Cauchy–Green strain tensor, in terms of the current Cartesian coordinates (x, y, z), is equal to

$$\mathbf{B} = \begin{bmatrix} 2A^2ax & 0 & 0 \\ 0 & \dfrac{a}{(2x)} & 0 \\ 0 & 0 & \dfrac{1}{(A^2a^2)} \end{bmatrix}.$$

Then the non-zero components of the corresponding Cauchy stress tensor depend only on x [13, p. 189]

$$\sigma_{xx} = -p,$$

$$\sigma_{yy} = \sigma_{xx} + \beta_1\left(\frac{a}{2x} - 2A^2ax\right) + \beta_{-1}\left(\frac{2x}{a} - \frac{1}{2A^2ax}\right)$$

and

$$\sigma_{zz} = \sigma_{xx} + \beta_1\left(\frac{1}{A^2a^2} - 2A^2ax\right) + \beta_{-1}\left(A^2a^2 - \frac{1}{2A^2ax}\right).$$

(c) Stretching and twisting of an annular wedge

After the successive deformations (2.4) and (2.7), the left Cauchy–Green strain tensor, in terms of the current cylindrical polar coordinates (r, θ, z), takes the form

$$\mathbf{B} = \begin{bmatrix} a & 0 & 0 \\ 0 & a + \dfrac{\tau^2r^2}{a^2} & \dfrac{\tau r}{a^2} \\ 0 & \dfrac{\tau r}{a^2} & \dfrac{1}{a^2} \end{bmatrix}.$$

Then the non-zero components of the associated Cauchy stress tensor depend only on r [13, p. 190]

$$\sigma_{rr} = \frac{\tau^2}{a^2}\int \beta_1 r\,\mathrm{d}r, \quad \sigma_{\theta\theta} = \sigma_{rr} + \beta_1 r^2\frac{\tau^2}{a^2},$$

$$\sigma_{\theta z} = r\frac{\tau}{a}\left(\frac{\beta_1}{a} - \beta_{-1}\right) \quad \text{and} \quad \sigma_{zz} = \sigma_{rr} - \beta_1 a\left(1 - \frac{1}{a^3}\right) + \frac{\beta_{-1}}{a}(a^3 - 1) - \beta_{-1}r^2\frac{\tau^2}{a}.$$

References

1. Weissengruber GE, Egger GF, Hutchinson JR, Groenewald HB, Elsässer L, Famini D, Forstenpointner G. 2006 The structure of the cushions in the feet of African elephants (*Loxodonta africana*). *J. Anat.* **206**, 781–792. (doi:10.1111/j.1469-7580.2006.00648.x)
2. Stover EL. 1951 *An introduction to the anatomy of seed plants*. Boston, MA: DC Heath and Co..
3. Alexander RMcN, Bennett MB, Ker RF. 1986 Mechanical properties and function of the paw pads of some mammals. *J. Zool. Lond. A* **209**, 405–419. (doi:10.1111/j.1469-7998.1986.tb03601.x)
4. Clercq DD, Aerts P, Kunnen M. 1994 The mechanical characteristics of the human heel pad during foot strike in running: an in vivo cineradiographic study. *J. Biomech.* **27**, 1213–1222. (doi:10.1016/0021-9290(94)90275-5)
5. Rome K. 1998 Mechanical properties of the heel pad: current theory and review of the literature. *Foot* **8**, 179–185. (doi:10.1016/S0958-2592(98)90026-8)

6. Bennett MB, Ker RF. 1990 The mechanical properties of the human subcalcaneal fat pad in compression. *J. Anat.* **171**, 131–138.
7. Napier J. 1993 *Hands*, revised edn. Princeton, NJ: Princeton University Press.
8. Jahss MH, Kummer F, Michelson JD. 1992 Investigations into the fat pads of the sole of the foot: heel pressure studies. *Foot Ankle* **131**, 227–232. (doi:10.1177/107110079201300501)Kuhn J G: Changes in elastic.
9. Ker RF. 1999 The design of soft collageneous load-bearing tissues. *J. Exp. Biol.* **202**, 3315–3324.
10. Ledoux WR, Blevins JJ. 2007 The compressive material properties of the plantar soft tissue. *J. Biomech.* **40**, 2975–2981. (doi:10.1016/j.jbiomech.2007.02.009)
11. Miller-Young JE, Duncan NA, Baroud G. 2002 Material properties of the human calcaneal fat pad in compression: experiment and theory. *J. Biomech.* **35**, 1523–1531. (doi:10.1016/S0021-9290(02)00090-8)
12. Natali AN, Fontanella CG, Carniel EL. 2012 A numerical model for investigating the mechanics of calcaneal fat pad region. *J. Mech. Behav. Biomed. Mater.* **5**, 216–223. (doi:10.1016/j.jmbbm.2011.08.025)
13. Truesdell C, Noll W. 2004 *The non-linear field theories of mechanics*, 3rd edn. Berlin, Germany: Springer.
14. Mihai LA, Goriely A. 2011 Positive or negative Poynting effect? The role of adscititious inequalities in hyperelastic materials. *Proc. R. Soc. A* **467**, 3633–3646. (doi:10.1098/rspa.2011.0281)
15. Mihai LA, Goriely A. 2014 Nonlinear Poisson effects in soft honeycombs. *Proc. R. Soc. A* **470**, 20140363. (doi:10.1098/rspa.2014.0363)
16. Scanlon. MG 2005 Biogenic cellular solids. In *Soft materials: structure and dynamics* (eds JR Dutcher, AG Marangoni), pp. 321–349. New York, NY: Marcel Dekker.
17. Gibson LJ, Ashby MF, Harley BA. 2010 *Cellular materials in nature and medicine*. Cambridge, UK: Cambridge University Press.
18. Baskin TI, Jensen OE. 2013 On the role of stress anisotropy in the growth of stems. *J. Exp. Bot.* **64**, 4697–4707. (doi:10.1093/jxb/ert176)
19. Rich PM. 1986 Mechanical architecture of arborescent rain forest palms. *Principes* **30**, 117–131.
20. Vandiver R, Goriely A. 2008 Tissue tension and axial growth of cylindrical structures in plants and elastic tissues. *Europhys. Lett.* **84**, 58004. (doi:10.1209/0295-5075/84/58004)
21. Warner M, Thiel BL, Donald AM. 2000 The elasticity and failure of fluid-filled cellular solids: theory and experiment. *Proc. Natl Acad. Sci. USA* **97**, 1370–1375. (doi:10.1073/pnas.020501797)
22. Gibson LJ, Ashby MF. 1997 *Cellular solids: structure and properties*, 2nd edn. Cambridge, UK: Cambridge University Press.
23. Weaire D, Fortes MA. 1994 Stress and strain in liquid and solid foams. *Adv. Phys.* **43**, 685–738. (doi:10.1080/00018739400101549)
24. Green AE, Adkins JE. 1970 *Large elastic deformations* (*and non-linear continuum mechanics*), 2nd edn. Oxford, UK: Oxford University Press.
25. Green AE, Zerna W. 1968 *Theoretical elasticity*, 2nd edn. Oxford, UK: Clarendon Press.
26. Ogden RW. 1997 *Non-linear elastic deformations*, 2nd edn. New York, NY: Dover.
27. Wells PNT, Liang H-D. 2011 Medical ultrasound: imaging of soft tissue strain and elasticity. *J. R. Soc. Interface* **8**, 1521–1549. (doi:10.1098/rsif.2011.0054)
28. Maas SA, Ellis BJ, Ateshian GA, Weiss JA. 2012 FEBio: finite elements for biomechanics. *J. Biomech. Eng.* **134**, 011005. (doi:10.1115/1.4005694)
29. Melnik AV, Borja Da Rocha H, Goriely A. In press. On the modeling of fiber dispersion in fiber-reinforced elastic materials. *Int. J. Nonlinear Mech.* (doi:10.1016/j.ijnonlinmec.2014.10.006)